Hindawi
International Journal of Antennas and Propagation
Volume 2022, Article ID 8233597, 10 pages
https://doi.org/10.1155/2022/8233597

Research Article

A High-Efficiency Microstrip Antenna Pair with Similar Pi-Shaped Decoupling Structure for 3.5 GHz 5G Ultrathin Smartphones

Di Wu, Yang Qiu, Guoliang Yu, Mingmin Zhu, and Hao-Miao Zhou

Key Laboratory of Electromagnetic Wave Information Technology and Metrology of Zhejiang Province, College of Information Engineering, China Jiliang University, Hangzhou 310018, China

Correspondence should be addressed to Mingmin Zhu; mzhu@cjlu.edu.cn and Hao-Miao Zhou; zhouhm@cjlu.edu.cn

Received 1 August 2022; Revised 5 November 2022; Accepted 11 November 2022; Published 21 November 2022

Academic Editor: Khaled Rouabah

In this paper, a low profile and high-efficiency decoupling antenna pair for multiunit smartphones is proposed using a similar π-shaped feed structure that can excite the dipole radiation mode of microstrip antenna. Ordinarily, symmetrical single-port T-shaped microstrip antennas can only excite monopole modes of bilateral radiation. This paper changes the vertical feeding microstrip structure into two oblique, similar π-shaped feeding structures. This oblique feeding structure can excite the dipole mode of unilateral radiation of the microstrip antenna. Using this method, the antenna design can be simplified, and the low-coupling independent radiation on both sides of the microstrip antenna can be freely controlled without the need for additional structures. Considering the ultra-thin characteristics of 5G smartphone devices, the parameters of the antenna are further optimized: the optimized antenna profile is only 3.7 mm. The measured results show that the 2×2 microstrip antenna pairs can effectively cover the 3.5 GHz band (3.4–3.6 GHz), with a coupling that varies from −16.14 dB to −11.01 dB and an efficiency that varies from 80% to 94.1%. The 8×8 MIMO smartphone antenna results show that the coupling varies from −20.1 dB to −12.17 dB, the efficiency varies from 79.72% to 93.7%, and the envelope correlation coefficient (ECC) is lower than 0.05. The microstrip antenna decoupling pair with a similar π-shaped feed structure proposed in this paper has high efficiency and low-profile characteristics have important application value in the decoupling design of 3.5 GHz 5G ultra-thin smartphone antennas.

1. Introduction

With constant advancements in mobile communication technology, the requirements for antennas in handheld mobile devices are constantly increasing. The fifth-generation mobile communication system (5G) has been commercially available since 2020; the frequency band of 5G smartphone antennas mainly operates in the sub-6 GHz and millimeter-wave (mm W) bands [1, 2]. To realize super-large-capacity data transmission, multiple-input multiple-output (MIMO) systems are usually required [3, 4]. The mainstream trend for 5G smartphone antennas in the sub-6 GHz band involves adopting 8×8 MIMO antenna structures. For each antenna unit to send and receive signals normally, very low envelope correlation coefficients and very low port-to-port coupling are required [5, 6]. Therefore, in smartphones—especially ultra-thin smartphones—designing miniaturized MIMO antennas in a very limited space is crucial, along with making each antenna unit have good isolation and excellent performance.

At present, the coupling between antenna units in MIMO smartphone antennas is a key issue. There have been many studies on decoupling methods between multiunit antennas, such as defective ground or neutral line structures [7, 8], external lumped components [9, 10], pattern diversity [11, 12], etc. Recently, researchers found that simultaneously feeding a shared radiator with two ports can make full use of antenna resources and reduce the complexity of the antenna structure [13, 14]. More importantly, the shared radiator antenna has significant advantages in terms of reducing coupling [15–17]. Sun et al. proposed a broadband shared radiator structure for a rectangular patch smartphone antenna, which realizes decoupling at broadband 3.3–4.2 GHz by adjusting the position of the feed point [18]. However, the

profile of the rectangular patch is 7.5 mm, which is not suitable for phone devices with ultra-thin screens. When the profile height of the antenna is relatively low, using the general decoupling method may lead to the deterioration of the bandwidth and efficiency of the original antenna. For example, Deng et al. [9] designed a low-profile antenna unit and used lumped elements to reduce the coupling between the units. The bandwidth of the antenna unit before decoupling is 3.25–3.63 GHz, and the coupling is less than −4 dB. After decoupling, the bandwidth becomes 3.42–3.58 GHz, the coupling is less than −12.4 dB, and the efficiency varies from 37.6% to 50.7%. The use of lumped-component decoupling leads to a significant decline in the bandwidth and efficiency of the antenna. According to Deng et al. [11], using the decoupling method of connecting feed points can obtain good isolation and efficiency, but the overall size of the antenna will increase by about 7 mm × 25 mm, which is not suitable for integrated phone devices. Therefore, the decoupling design of a low-profile antenna with excellent comprehensive performance still has important application prospects in future 5G ultra-thin smartphone devices.

Aimed at the problems of large unit size, high profile, and low efficiency of existing 5G smartphone antennas, a microstrip antenna decoupling pair using a similar π-shaped feed structure is proposed in this paper. First, a single-port T-shaped microstrip antenna is designed on the long edge of a 150 mm × 75 mm metal ground. Next, the vertical feed microstrip is bent to the left and right, such that it subtends a certain angle with the ground plane. This new feeding structure provides an asymmetrical flow path for the current on the antenna surface and excites a dipole resonance mode that is absent in the T-shaped structure, while the other side does not have this resonance mode. In the new resonant mode, the independent radiation of the T-shaped antenna arms is controlled according to the bending direction of the feeding microstrip. The length of the optimized 2 × 2 microstrip antenna pair is 32.4 mm, and the folded profile is only 3.7 mm. The experimental measurement results show that the port coupling is lower than −11 dB on the 3.5 GHz band (3.4–3.6 GHz). Then, an eight-unit 5G MIMO smartphone antenna is proposed based on a dual-port microstrip antenna pair. The measured results show that the port coupling is lower than −12.17 dB and the efficiency varies from 79.72% to 93.7%. The proposed antenna pair model fed by a similar π-shaped feed structure has a good application prospect, and the final eight-unit 5G MIMO smartphone antenna has an excellent performance in terms of low coupling, small size, low profile, and high efficiency.

2. Decoupling Principle of the Microstrip Antenna Pair Fed by a Similar Pi-Shaped Feed Structure

The use of T-shaped antennas has natural advantages over using two separate 1/4-times-wavelength monopole antennas. The dual monopoles of the T-shaped antenna are fed together by a single port, which reduces the ground clearance and helps realize miniaturization. However, each arm of the asymmetrical T-shaped antennas is a monopole antenna, and the entire structure can be spatially viewed as a dual-unit radiation structure with only one feed port; therefore, this dual-unit cannot radiate independently. Currently, in the design of most 5G smartphone antennas, multiple units' radiations are required to be controlled by multiple ports, and the coupling between radiation units needs to be reduced to −10 dB. Therefore, it is crucial to realize a dual-port MIMO antenna where the bilaterals of the T-shaped antenna can independently excite their radiation.

The surface current distribution obtained through the simulation and the equivalent resonant circuit of a single-port T-shaped antenna are shown in Figure 1(a). When the port is excited, the current flow directions in the arms of the symmetrical T-shaped antenna are opposite, as is that of the ground plate edge below. Because the current direction on the feed microstrip connected to the port is downward, both the left and right sides of the antenna form a current-resonant circuit. Therefore, radiation is generated on both sides, and the distribution is symmetrical (see the two red circles in Figure 1(a)). This radiation can be determined to be monopole radiation from the current distribution. The vertical feed microstrip, which acts as a connecting hub, plays a key role in the radiation of the antenna arms. Therefore, it is entirely possible to achieve independent bilateral radiation by changing the feed structure.

The new structure of the improved T-shaped antenna is shown in Figure 1(b), obtained by bending the feed microstrip to the left. As can be seen, the current direction in both arms still opposes that on the edge of the floor; however, both arms have the same current direction in this event. The current in the improved feed microstrip structure flows to the floor, so a current-resonant circuit is formed on the left side of the antenna; on the right side of the antenna, because the current direction in the feed microstrip opposes the current direction in the loop, no resonance is generated. From the current distribution, it can be seen that the radiation from the left side of the antenna is dipole radiation. Therefore, it can be concluded that when the feed microstrip in Figure 1(b) is bent to the left, the T-shaped antenna can control the left arm's radiation by exciting the dipole resonance mode. Similarly, if the feed microstrip is bent to the right, the radiation of the right arm of the T-shaped antenna can also be controlled. According to these radiation characteristics, a microstrip antenna decoupling pair prototype using a similar π-shaped feed structure can be proposed, as shown in Figure 1(c). There are two bent feed microstrips, which are symmetrically placed. When port 1 is excited, the left arm excites the dipole resonance mode while the right arm does not. Similarly, when port 2 is excited, the right arm excites the dipole resonance mode, while the left arm does not. It is clear that exciting an independent dipole resonance mode on a single arm of the microstrip antenna pair is of great value to the current design of MIMO smartphone antennas for the 5G band, which can achieve the design of low-profile MIMO antennas based on similar π-shaped feed decoupling structures.

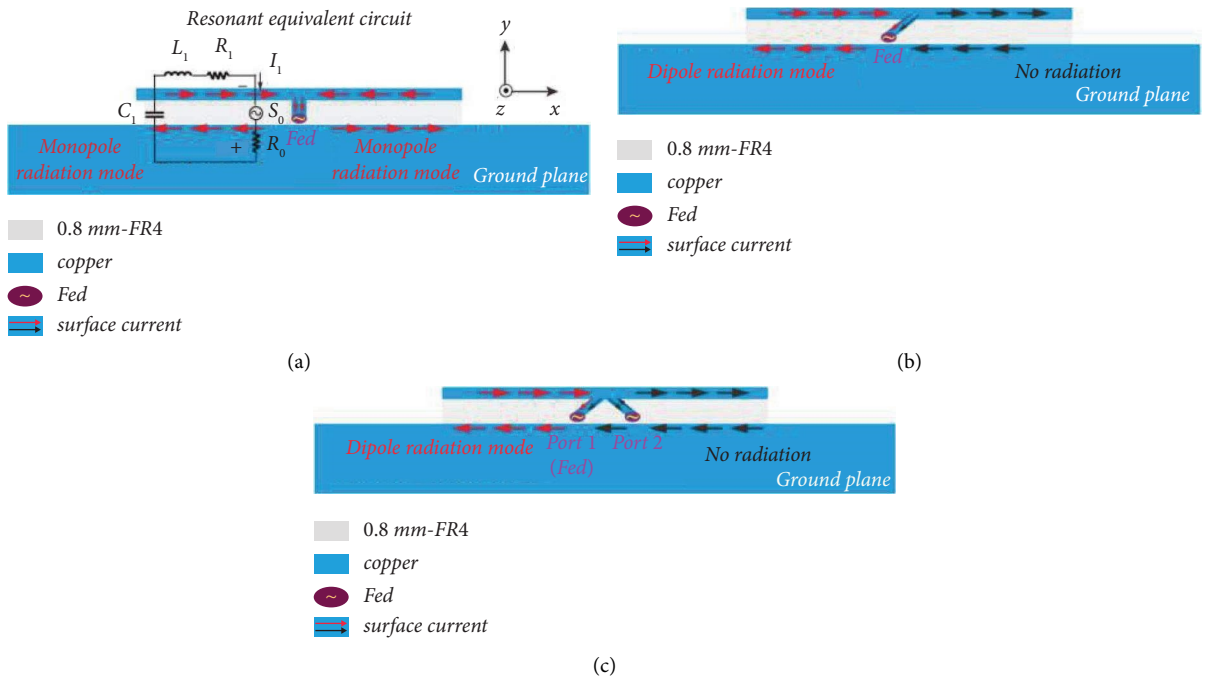

FIGURE 1: Current distribution of. (a) The single-port T-shaped antenna A. (b) The single-port deformed T-shaped antenna B with oblique microstrip. (c) The dual-port deformed T-shaped antenna C with two oblique microstrips excited by port 1 (unit: mm).

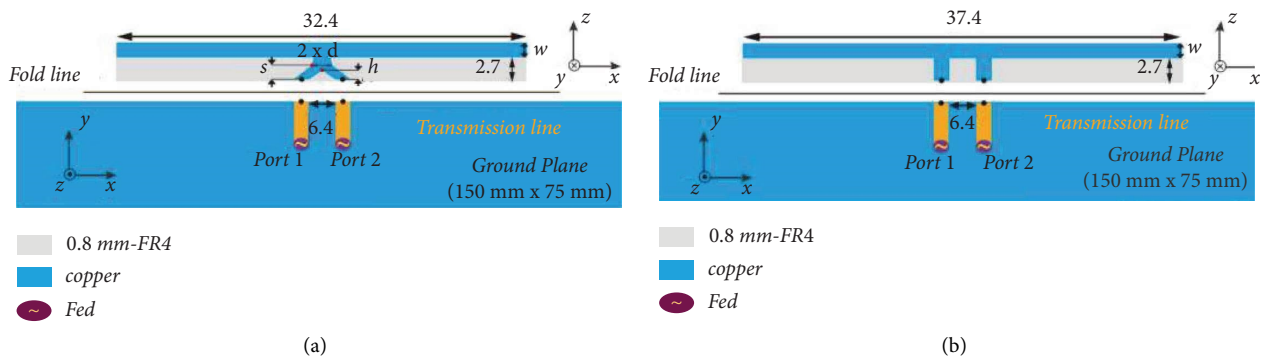

FIGURE 2: Geometry of. (a) The proposed dual-port microstrip antenna pair fed by a similar π-shaped feeding structure. (b) The compared dual microstrip antenna pair fed by a feeding structure with connecting line (unit: mm).

The electrical dimensions of the microstrip antenna pair in Figure 1(c) are adjusted to operate on the 3.5 GHz band (3.4–3.6 GHz) and to optimize its structure. The main adjusted parameters are d, s, and h, which are related to the shape of the feed structure, and the parameter w is related to the width of the microstrip (see Figure 2(a)). The antenna is mainly used in ultra-thin smartphones, so it is designed on FR-4 ($\varepsilon_r = 4.4$ and $\tan\delta = 0.02$), with a size of 150 mm × 75 mm × 0.8 mm. The antenna is folded 90° along the edge of the substrate to achieve 0 clearances. To facilitate feeding, 4 mm × 2 mm long microstrip transmission lines are used to connect the ports of the antenna to the feeders. The optimum simulation model of the antenna is shown in Figure 2(a). In addition, to demonstrate the advantages of the proposed similar π-shaped feeding structure in the miniaturization of low-profile microstrip antenna pairs, a microstrip antenna pair directly fed by the feed structure with the connecting line is selected as a comparison model, as shown in Figure 2(b). The connecting line of the vertical feeding structure in Figure 2(b) increases the electrical dimension length of the dipole radiation mode of the microstrip antenna. Therefore, when covering the same operating bandwidth (the 3.5 GHz band (3.4–3.6 GHz)), the comparison model shown in Figure 2(b) requires a microstrip length of 37.4 mm, whereas the model proposed in Figure 2(a) only needs a microstrip length of 32.4 mm. This is because the length of the electrical dimension of the microstrip antenna is related to the length of the current path on the microstrip. When the proposed microstrip antenna model excites a dipole radiation mode, the current

path length on the antenna is the equivalent distance from the horizontal microstrip endpoint to the feeding endpoint. Since the two antenna pairs in Figures 2(a) and 2(b) have the same profile height, when the antenna feed port distance is kept constant, using the vertical strip structure on the headroom (Figure 2(b)) reduces the equivalent distance from the horizontal microstrip endpoint to the feed endpoint compared to the similar π-shaped feed structure (Figure 2(a)). Therefore, if the antenna operating frequencies of the structures shown in Figures 2(a) and 2(b) are kept the same, the use of the vertical strip structure (Figure 2(b)) must increase the length of the horizontal microstrip and, consequently, increase the electrical size of the microstrip antenna.

Next, the S parameters of the antenna are simulated. In the simulation, port 1 is set to "excitation," and port 2 is set to a "50 Ω match-terminator." The optimization results of each parameter are shown in Figure 3(a). It can be seen that the larger the width w of the microstrip, the better the coupling of the antenna; however, the resonance depth simultaneously decreases. The lower the height h between the two feed microstrips, the better is the effective coupling bandwidth (see Figure 3(b)). The parameters d and s have the greatest influence on S_{11}. The larger the parameter value, the higher the resonance depth of the antenna, and the worse the coupling depth and bandwidth. Based on the results shown in Figure 3, the parameters $w = 1$ mm, $h = 12$ mm, $d = 1.8$ mm, and $s = 1.5$ mm are determined, and the overall size of the antenna is found to be 32.4 mm × 3.7 mm. The simulation results of the S-parameter when using the microstrip antenna pair of the similar π-shaped feed structure shown in Figure 2(a) and the feed structure with the connecting line shown in Figure 2(b), are compared as shown in the left coordinate of Figure 4. It can be seen that, in the near field, the decoupling results of $S11$ and $S21$ using the vertical feed structure are very poor. Therefore, using the vertical feed structure will not only occupy a larger antenna design space but also reduce the antenna's impedance matching and decoupling effect. The far-field decoupling results (i.e., ECC) of the microstrip antenna with the two feed structures are shown on the right coordinate in Figure 4. It can be seen that, in the far field, the ECCS of the antenna pairs decoupled using the vertical feed structure are high, and the decoupling effect is poor. In contrast, the ECCS of the antenna pairs decoupled using the proposed similar π-shaped feed structure are lower. In conclusion, using the proposed similar π-shaped feed structure has significant advantages in terms of both near-field and far-field performance.

3. Simulation and Measurement Results of Microstrip Antenna Pairs Fed by Similar Pi-Shaped Feed Structures

Based on the decoupling principle of the microstrip antenna pairs fed by a similar π-shaped feed decoupling structure proposed in Section 2, the antenna operates on the 3.5 GHz band (3.4–3.6 GHz), and the antenna structure with the substrate is obtained, as shown in Figure 5(a). The far-field radiation pattern and surface current distribution of the antenna at 3.5 GHz are simulated using the high-frequency electromagnetic field simulation software ANSOFT HFSS, as shown in Figures 5(b)–5(e). Figures 5(b) and 5(c) show that that when port1 is excited, the antenna emits a radiating hemisphere on the left and almost no radiation on the right. As described in Figure 1(c) in Section 2, the reason for this radiation is that there is a strong loop current distribution on the left side of the microstrip antenna pair, while the right half will not produce a strong loop current because of the current cancellation principle. Similarly, when port 2 is fed, the antenna has a right radiation hemisphere, and almost no radiation is generated on the left.

The antenna in Figure 3 is fabricated and experimentally measured; its ports are individually fed by a semiflexible coaxial line operating at a frequency of 0–6 GHz. The S-parameters are obtained using an Agilent N5230C vector network analyzer. The results are shown in Figure 6(a). The −6 dB operating frequency band of the simulated S_{11} is lower than 3.63 GHz, while the experimentally measured S_{11} operating frequency band is less than 3.87 GHz; therefore, the measured results are better than the simulated results. The minimum value of the simulated S_{21} is −12.71 dB, and the −10 dB bandwidth is 3.37–3.61 GHz. The minimum value of S_{21} measured experimentally is −16.14 dB, and the −10 dB bandwidth is 3.37–3.67 GHz. In general, the experimental results for S_{11} and S_{21} are consistent with the simulation results and meet the design requirements. The total far-field radiation efficiency of the antenna is measured in a microwave anechoic chamber, and the results are shown in Figure 6(b). The antenna does not have any additional lossy components and, therefore, exhibits good performance in the far field. It can be seen from the figure that the efficiency is more than 80%, with a maximum efficiency of 94%, and the gain is more than 4.7 dB at 3.4–3.6 GHz.

4. Eight-Unit Antenna Design

According to the design and analysis of the dual-port microstrip antenna pair above, an 8 × 8 MIMO antenna structure for a 5G smartphone is proposed; a geometric diagram is shown in Figure 7(a). Four identical pairs of antennas are arranged with a size of 150 mm × 75 mm on both long sides of the substrate. On each long side, the shortest distance between the microstrip antenna pair edge and the structural edge is 37 mm, the bottom dielectric material is a 0.8 mm thick FR4 substrate, and the overall structure is centrally symmetrical. Figures 7(b) and 7(c) show the actual production model of the eight-element antenna structure. The antenna has a total of eight ports, each of which is fed by a semiflexible coaxial line operating at a frequency of 0–6 GHz.

The S parameters of the eight-unit antenna are simulated and measured experimentally; the results are shown in Figure 8(a). During the experimental measurement, the ports of the vector network analyzer are connected to the ports of the microstrip antenna pairs, and the remaining six ports are connected to a 50 Ω match-terminator. As can be seen from the figure, the −6 dB bandwidth of the simulated S_{11} is a wideband of less than 3.64 GHz, while the measured bandwidth is a

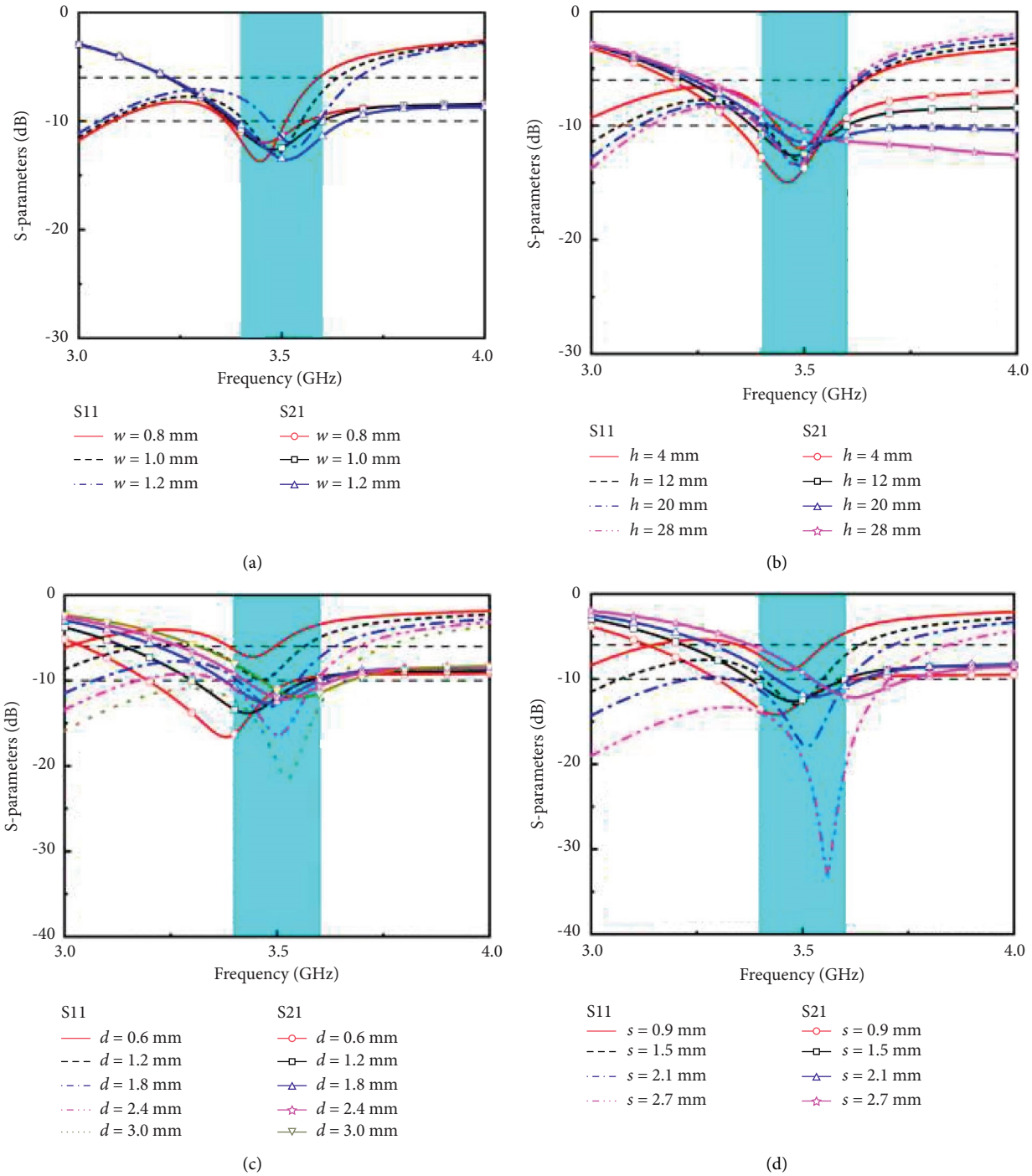

Figure 3: Simulated S-parameters of the dual-port microstrip antenna pair with different values of (a) w. (b) h. (c) d. (d) s.

wideband of less than 3.86 GHz. The −6 dB bandwidth of the simulated S_{22} is a wideband of less than 3.64 GHz, while the measured bandwidth is a wideband of less than 3.79 GHz. The −10 dB bandwidth of the simulated S_{21} is 3.36–3.64 GHz, and the maximum depth can reach −14.23 dB. The measured S_{21} bandwidth is 3.35–3.68 GHz, and the maximum depth is −20.1 dB. On the operating frequency band of 3.4–3.6 GHz, the simulated S_{21} is lower than −11.6 dB, and the measured result is lower than −12.2 dB. The measured coupling results between other units of the antenna are shown in Figure 7(b). Since the distance between Ant.2 and Ant.3 is only 37 mm, the coupling between them is slightly higher, and the measured results at 3.4–3.6 GHz are less than −14.1 dB. The coupling between the remaining units is maintained at a very low level, which does not greatly impact the units' radiation.

Since the antenna structure is highly symmetrical, only the far-field performances of Ant.1 and Ant.2 are tested. The total gain and efficiency measured in the microwave anechoic

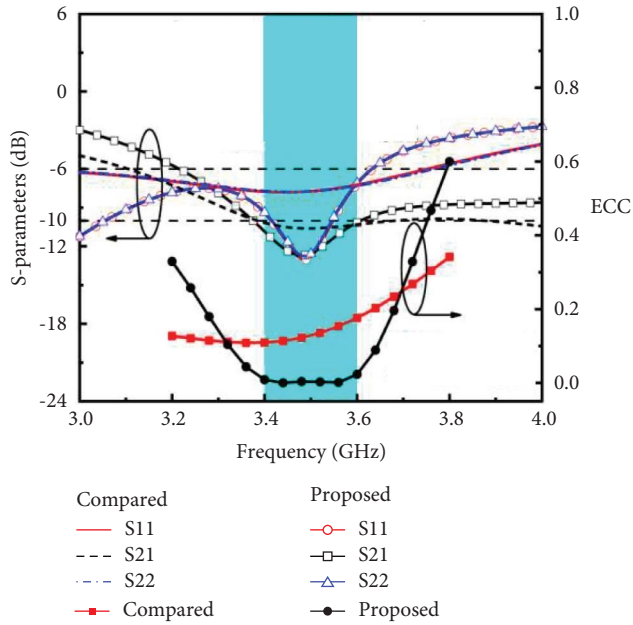

Figure 4: Simulated S-parameters and ECC of the proposed dual-port microstrip antenna pair fed by a similar π-shaped structure and the compared dual microstrip antenna pair fed by feeding structure with the connecting line.

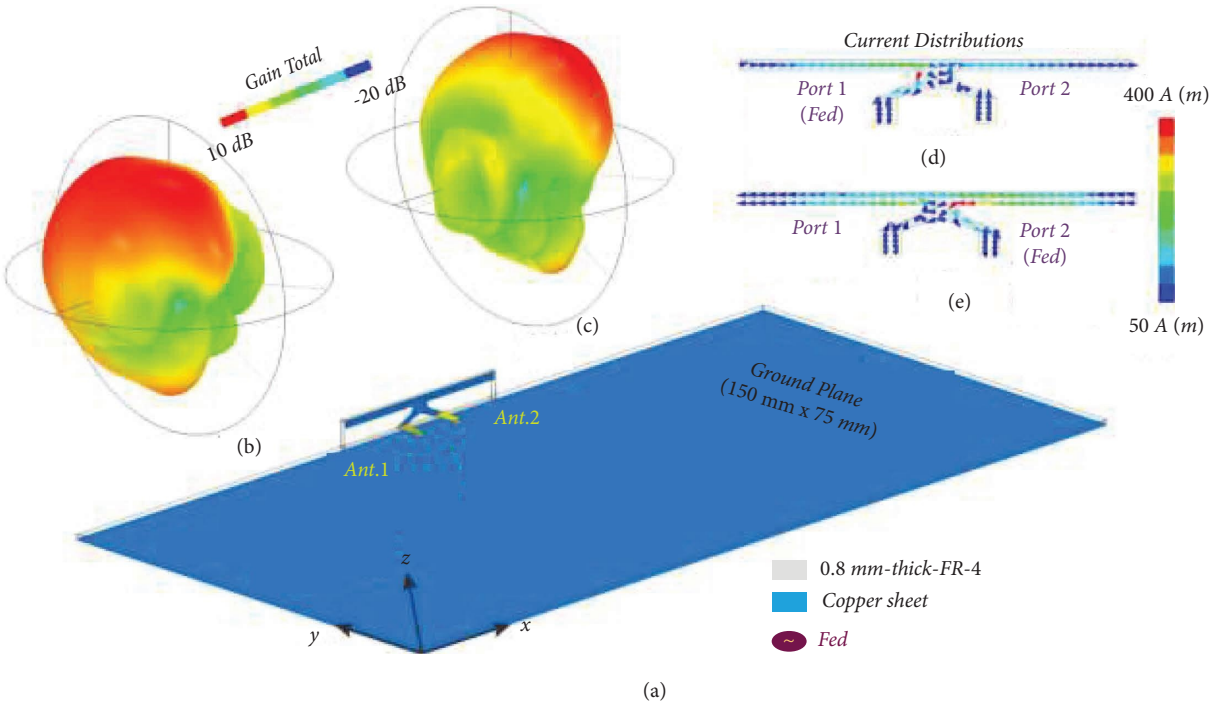

Figure 5: (a) Overall view of the dual-port microstrip antenna pair. The far-field radiation pattern of the dual-port microstrip antenna pair at 3.5 GHz. (b) When port 1 is excited. (c) When port 2 is excited. Surface current distributions are at 3.5 GHz. (d) When port 1 is excited. (e) When port 2 is excited.

chamber are shown in Figures 8(c) and 8(d). During measurement, the measured antenna element is connected to the test port, and the other seven ports are connected to the 50 Ω match-terminators. At 3.4–3.6 GHz, the efficiency of Ant.1 varies from 79.72% to 93.7%, and the efficiency of Ant.2 varies from 83.24% to 91.68%. The right coordinate of Figure 8(c) is the simulated ECC results. It can be seen that the gains of both units are greater than 4 dB and the ECCS of both Ant.1 and Ant.2 are less than 0.02; the final radiation performance is maintained at a high level. The far-field radiation performance of Ant.2 is slightly lower than that of Ant.1. This makes it clear that, in comparison to the dual-port antenna pair Ant.2 and

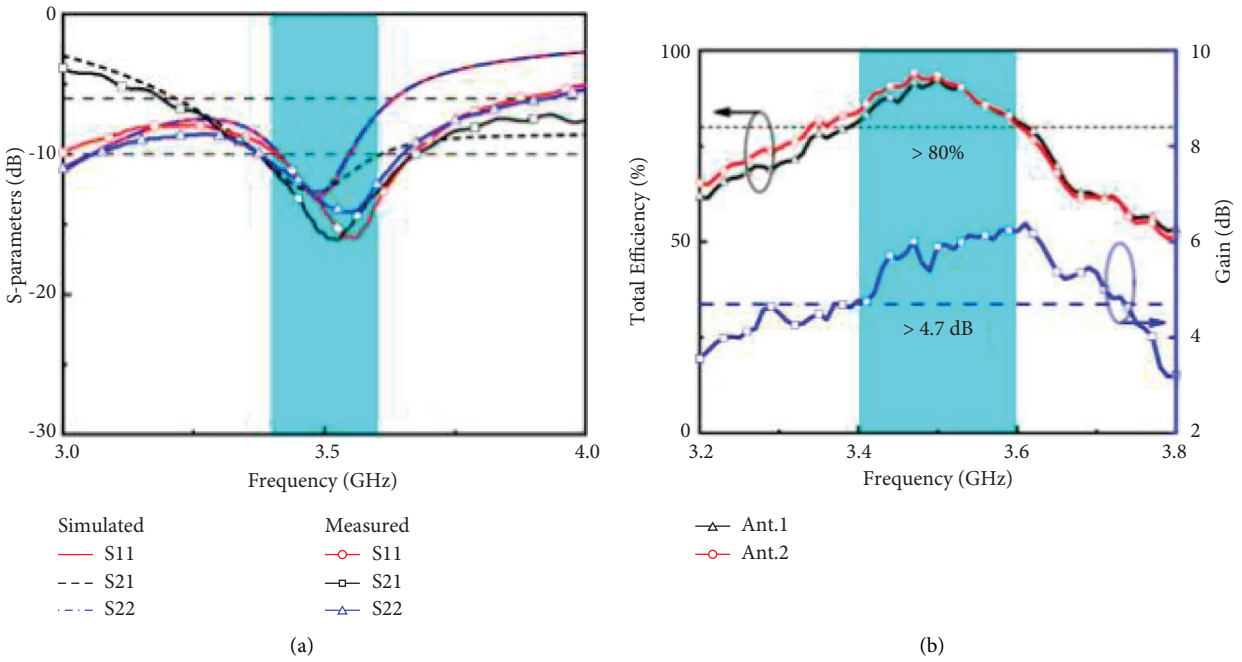

FIGURE 6: (a) Simulated and measured *S*-parameters. (b) Measured the total efficiency and gain of the dual-port microstrip antenna pair.

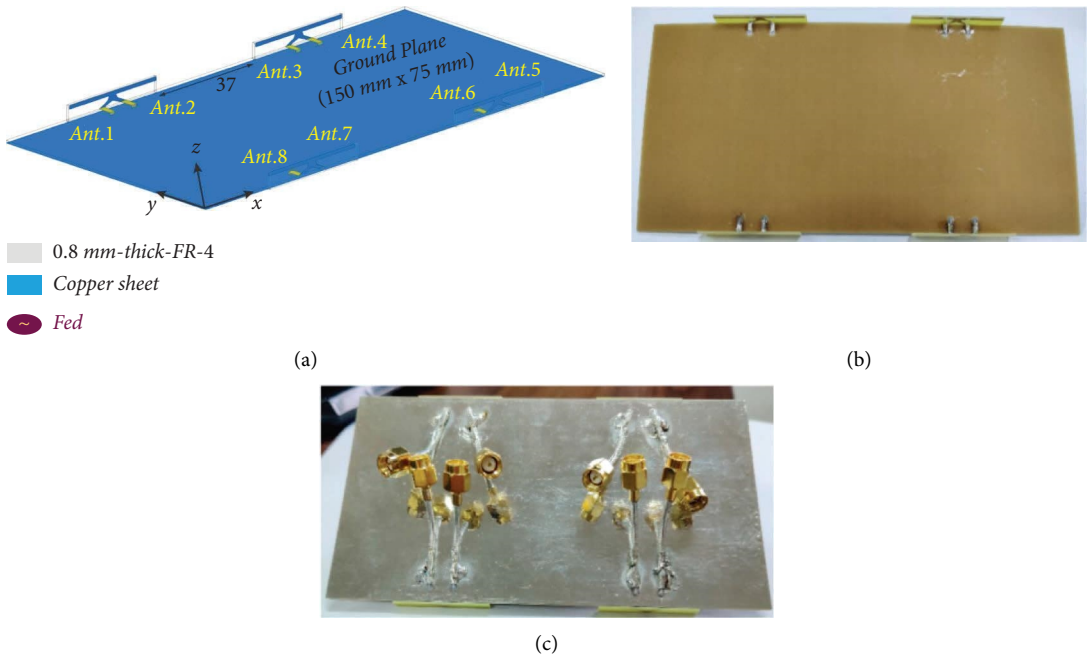

FIGURE 7: (a) Geometry of the proposed 8 × 8 MIMO antenna. Photographs of the proposed 8 × 8 MIMO antenna are included. (b) Top view. (c) Bottom view (unit: mm).

Ant.3, Ant.6 and Ant.7 are near the middle of the eight-unit antennas, whose efficiency and gain will decrease slightly due to their close distance and no decoupling method; however, their final radiation performance will remain at a very high level. The far-field correlation between Ant.1 and Ant.2 can be calculated from the far-field directivity coefficients measured in the darkroom. Here, the wireless channel is assumed to be isotropic. This can be formalized as follows [11]:

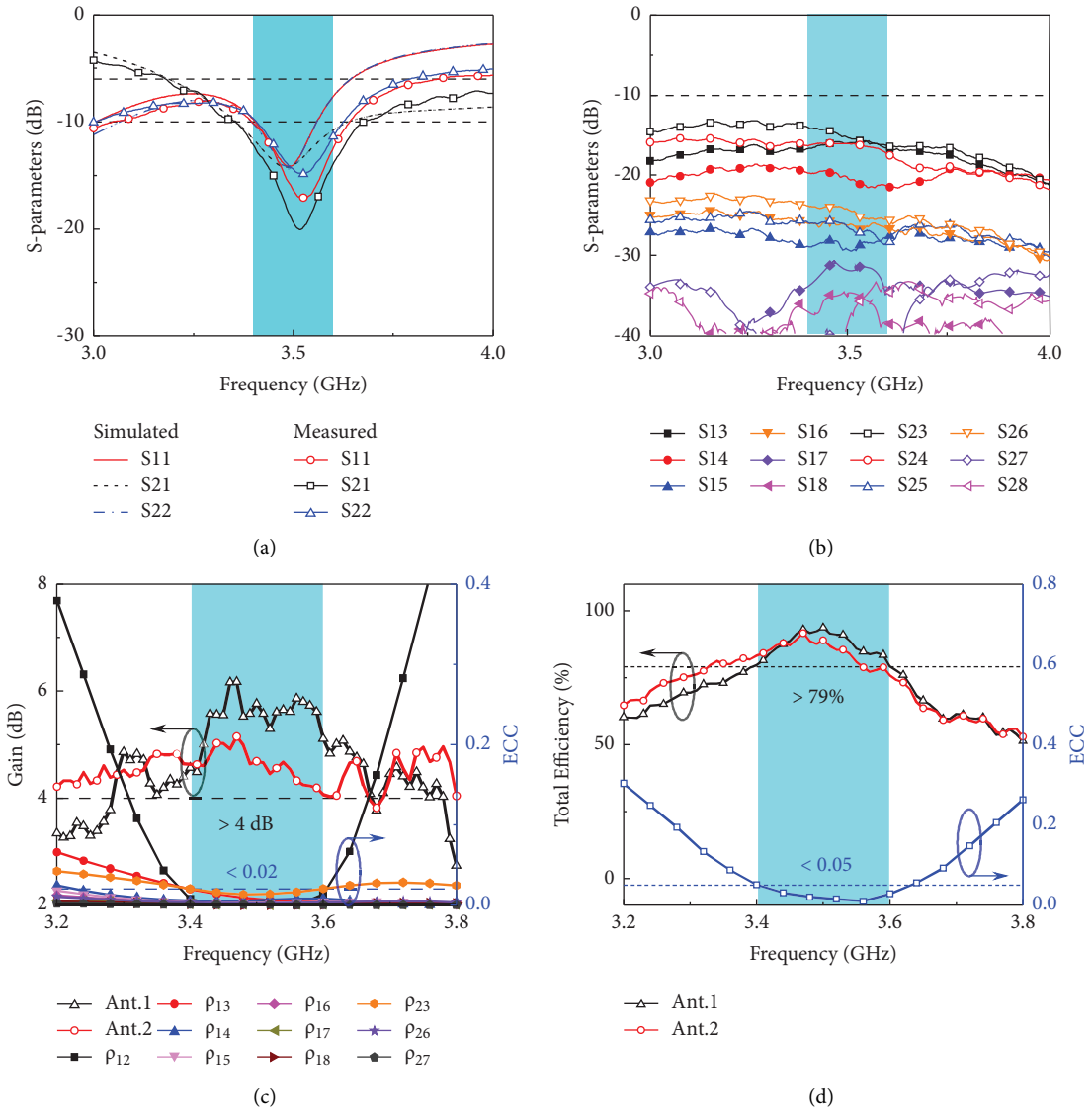

FIGURE 8: (a), (b) Simulated and measured *S*-parameters of the proposed 8 × 8 MIMO antenna; (c), (d) measured total gain, simulated ECC between different units, efficiency, and the calculated ECC of Ant.1 and Ant.2 in the proposed 8 × 8 MIMO antenna.

$$\rho_{12} = \frac{\int_{4\pi} \left| \overrightarrow{E_1}(\theta,\varphi) \cdot \overrightarrow{E_2^*}(\theta,\varphi) \right|^2 d\Omega}{\int_{4\pi} \left| \overrightarrow{E_1}(\theta,\varphi) \right|^2 d\Omega \cdot \int_{4\pi} \left| \overrightarrow{E_2}(\theta,\varphi) \right|^2 d\Omega}, \quad (1)$$

where ρ_{12} is the envelope correlation coefficient (ECC), $\overrightarrow{E_i}(\theta,\varphi)$ is the complex far-field radiation pattern when port i is excited, and Ω is the solid angle.

As shown in Figure 8(d), the calculated ECC is less than 0.05 at 3.4–3.6 GHz, indicating that the electromagnetic waves radiated by the two units have a very low spatial correlation.

Figure 9 presents the measured 2-D far-field patterns of Ant.1 and Ant.2 at 3.4, 3.5, and 3.6 GHz in the x-z ($\varphi = 90^\circ$) and x-y ($\theta = 0^\circ$) planes. From the curve shape of the coordinate planes in the figure, it can be seen that the radiation of Ant.1 is mainly in the negative direction of the x-axis, while that of Ant.2 is mainly in the positive direction of the x-axis. When two ports on the shared radiator are excited at the same time, the radiation of the two symmetrical hemispheres in the far field will not interfere with each other, which can ensure the omni-directivity of the radiation signal.

A comparison between the microstrip antenna with a similar π-shaped feed structure proposed in this paper and existing 5G antennas operating in the same bandwidth using the decoupled method is shown in Table 1. The proposed antenna area is only 32.4 mm × 3.7 mm, which is better than that of all compared antennas. Furthermore, the antenna has a 3.7 mm profile, which has obvious advantages as a low-profile antenna and is more suitable for ultra-thin smartphone devices. In addition, the efficiency of the antenna is higher than that of all comparative references. However, this antenna pair has no obvious advantage in terms of isolation. This is mainly because the decoupling method proposed in this paper is primarily suitable for low-profile mobile phone antennas. In comparison to the isolation in Deng et al. [11] (13.5 dB), which also describes a low-profile decoupling

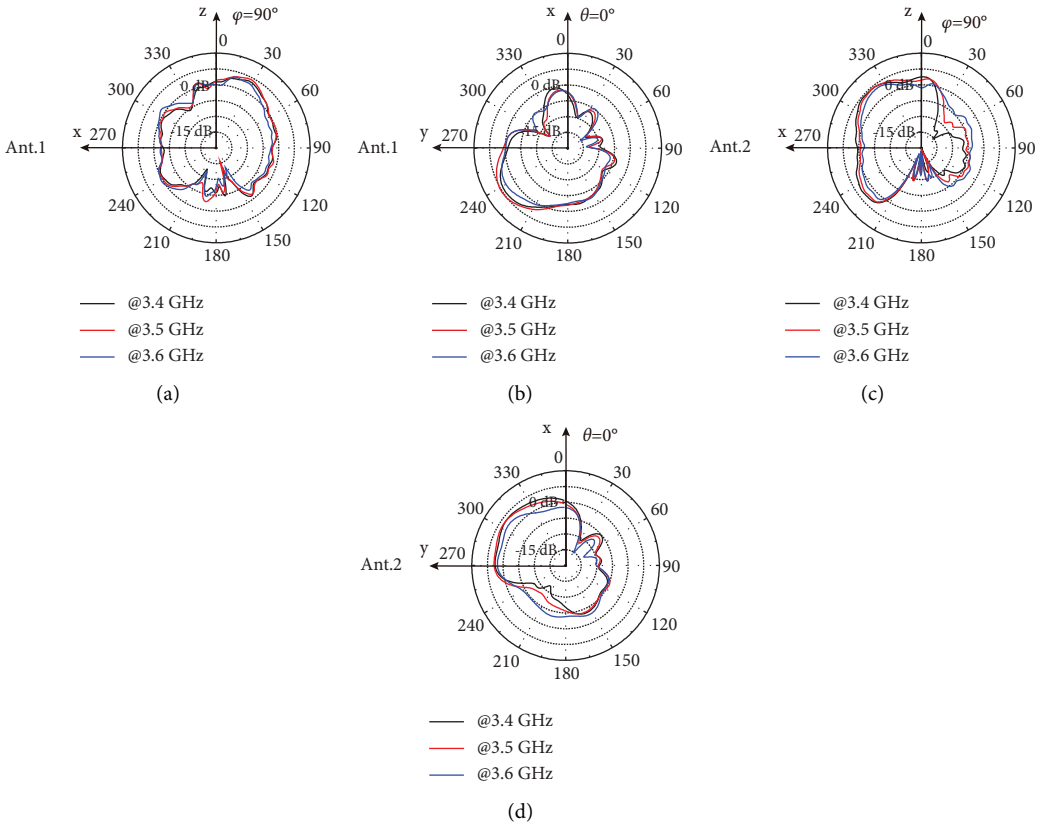

Figure 9: Measured radiation patterns of Ant.1 and Ant.2 in (a), (c) *x-z* planes, (b), (d) *x-y* planes.

Table 1: Comparison with existing works.

Reference	Size (mm^3)	Bandwidth	Isolation (dB)	Efficiency
[8]	$15 \times 7 \times 1$	3.34–3.65 GHz	15.0	>64%
[9]	$25 \times 10.5 \times 0.8$	3.33–3.67 GHz	14.0	>52%
[11]	$38.2 \times 3.2 \times 0.8$	3.42–3.59 GHz	13.5	>37.6%
[19]	$20 \times 6.2 \times 0.8$	3.38–3.63 GHz	17.0	>58%
[20]	$12 \times 6.5 \times 0.8$	3.4–3.6 GHz	10.0	>63%
This work	$32.4 \times 3.7 \times 0.8$	3.35–3.67 GHz	12.2	>79%

design, the design in this paper is 12.2 dB. However, the efficiency of Deng et al. [11] is just greater than 37.6%, and the proposed antenna has significant advantages in terms of efficiency. Although the isolation effect is better in Piao et al. [8], Deng et al. [9], and Ren et al. [19], the profiles of these antennas are relatively high, and their decoupling methods may not be suitable for low-profile antennas. Due to the limited design space of the low-profile antenna, it is very difficult to adjust the mutual impedance between the antenna units. Therefore, in comparison to the higher-profile antenna units, the decoupling effect of the low-profile antenna is more difficult to improve. In conclusion, in comparison to the existing antennas of the same kind, the antenna proposed in this paper is very competitive for use in smartphone devices and more in line with the trends of antenna miniaturization, low-profile characteristics, and multiunit application.

5. Conclusion

In this paper, a low-profile and high-efficiency decoupled microstrip antenna pair model for future MIMO smartphone antennas is proposed by changing the feed structure of the microstrip antenna. The oblique type of feed structure used in the antenna pair provides a new path for the current on the metal microstrip, excites the dipole mode of the antenna, and enables the two ports of the antenna to control the bilateral radiation independently. The optimized antenna pair size is 32.4 mm × 3.7 mm × 0.8 mm, and the profile height is only 3.7 mm. The measurement results show that in the 3.35–3.67 GHz band, the coupling between the ports of the eight-unit MIMO antenna is less than −12.17 dB, the ECC is less than 0.05, and the average efficiency of the ports is about 87%. In comparison to the existing 5G antennas using the decoupling method operating in the same bandwidth, the proposed similar π-shaped feed structure microstrip antenna has the advantages of a small size, low profile, high efficiency, simple structure, no additional decoupling branches, no additional materials, and excellent overall performance.

Data Availability

The data used support the findings of this study are available from the corresponding author upon reasonable request.

Conflicts of Interest

The authors declare that they have no conflicts of interest.

Authors' Contributions

Di Wu and Yang Qiu contributed equally to this work.

Acknowledgments

This work was funded by the National Natural Science Foundation of China (Grant nos. 11972333, 11902316, and 51902300), as well as the Natural Science Foundation of Zhejiang Province (Grant nos. LZ19A020001, LQ19F010005, and LY21F010011). The authors would like to express their sincere appreciation for this support.

References

[1] S. Islam, M. Zada, and H. Yoo, "Low-pass filter based integrated 5G smartphone antenna for sub-6-GHz and mm-wave bands," *IEEE Transactions on Antennas and Propagation*, vol. 69, no. 9, pp. 5424–5436, 2021.

[2] Y. Hei, J. He, and w. Li, "Wideband decoupled 8-element MIMO antenna for 5G mobile terminal applications," *IEEE Antennas and Wireless Propagation Letters*, vol. 20, no. 8, pp. 1448–1452, 2021.

[3] F. Boccardi, R. W. Heath, A. Lozano, T. L. Marzetta, and P. Popovski, "Five disruptive technology directions for 5G," *IEEE Communications Magazine*, vol. 52, no. 2, pp. 74–80, 2014.

[4] K. S. Mohamed, M. Y. Alias, M. Roslee, and Y. M. Raji, "Towards green communication in 5G systems: survey on beamforming concept," *IET Communications*, vol. 15, no. 1, pp. 142–154, 2020.

[5] W. Hong, "Solving the 5G mobile antenna puzzle: assessing future directions for the 5G mobile antenna paradigm shift," *IEEE Microwave Magazine*, vol. 18, no. 7, pp. 86–102, 2017.

[6] E. Mihret and G. Haile, "4G, 5G, 6G, 7G and future mobile technologies," *J Comp Sci Info Technol*, vol. 9, no. 2, p. 75, 2021.

[7] W. Huey Shin, S. Kibria, and M. Tariqul Islam, "Hexa band mimo antenna with neutralization line for LTE mobile device application," *Microwave and Optical Technology Letters*, vol. 58, no. 5, pp. 1198–1204, 2016.

[8] H. Piao, Y. Jin, Y. Xu, and L. Qu, "MIMO ground-radiation antennas using a novel closed-decoupling-loop for 5G applications," *IEEE Access*, vol. 8, pp. 142714–142724, 2020.

[9] C. Deng, D. Liu, and X. Lv, "Tightly arranged four-element MIMO antennas for 5G mobile terminals," *IEEE Transactions on Antennas and Propagation*, vol. 67, no. 10, pp. 6353–6361, 2019.

[10] L. Zhao, L. K. Yeung, and K.-L. Wu, "A coupled resonator decoupling network for two-element compact antenna arrays in mobile terminals," *IEEE Transactions on Antennas and Propagation*, vol. 62, no. 5, pp. 2767–2776, 2014.

[11] Z. Xu and C. Deng, "High-Isolated MIMO antenna design based on pattern diversity for 5G mobile terminals," *IEEE Antennas and Wireless Propagation Letters*, vol. 19, no. 3, pp. 467–471, 2020.

[12] L. Chang, Y. Yu, K. Wei, and H. Wang, "Orthogonally polarized dual antenna pair with high isolation and balanced high performance for 5G MIMO smartphone," *IEEE Transactions on Antennas and Propagation*, vol. 68, no. 5, pp. 3487–3495, 2020.

[13] C. Y. Hsu, L. T. Hwang, F. S. Chang, S. M. Wang, and C. F. Liu, "Investigation of a single-plate π-shaped multiple-input-multiple-output antenna with enhanced port isolation for 5 GHz band applications," *IET Microwaves, Antennas & Propagation*, vol. 10, no. 5, pp. 553–560, 2016.

[14] A. ToktasToktas, E. Yigit, and A. SabanciKayabasi, "CFAR based morphological filter design to remove clutter from GB-SAR images: an application to real data," *Microwave and Optical Technology Letters*, vol. 59, no. 10, pp. 2685–2692, 2017.

[15] A. ChenChen, J. Zhang, and Y. ZhaoYin, "A dual-feed MIMO antenna pair with one shared radiator and two isolated ports for fifth generation mobile communication band," *International Journal of RF and Microwave Computer-Aided Engineering*, vol. 27, no. 9, Article ID e21146, 2017.

[16] L. Sun, Y. Li, Z. Zhang, and Z. Feng, "Wideband 5G MIMO antenna with integrated orthogonal-mode dual-antenna pairs for metal-rimmed smartphones," *IEEE Transactions on Antennas and Propagation*, vol. 68, no. 4, pp. 2494–2503, 2020.

[17] X.-T. Yuan, Z. Chen, T. Gu, and T. Yuan, "A wideband PIFA-pair-based MIMO antenna for 5G smartphones," *IEEE Antennas and Wireless Propagation Letters*, vol. 20, no. 3, pp. 371–375, 2021.

[18] L. Sun, Y. Li, Z. Zhang, and H. Wang, "Self-decoupled MIMO antenna pair with shared radiator for 5G smartphones," *IEEE Transactions on Antennas and Propagation*, vol. 68, no. 5, pp. 3423–3432, 2020.

[19] Z. Ren, A. Zhao, and S. Wu, "MIMO antenna with compact decoupled antenna pairs for 5G mobile terminals," *IEEE Antennas and Wireless Propagation Letters*, vol. 18, no. 7, pp. 1367–1371, 2019.

[20] S. S. Altarawneh, B Alshamaileh, M H Alshimaileh, L. SharawiXingXu, and Q. Xu, "Ten antenna array using a small footprint capacitive-coupled-shorted loop antenna for 3.5 GHz 5G smartphone applications," *IEEE Access*, vol. 9, pp. 33796–33810, 2021.